CrystEngComm

Controlling nanowire nucleation and growth with a negative substrate bias

Journal:	*CrystEngComm*
Manuscript ID	CE-ART-02-2016-000403.R1
Article Type:	Paper
Date Submitted by the Author:	18-Mar-2016
Complete List of Authors:	Ball, Jeremy; London South Bank University, School of Engineering Reehal, H; London South Bank University, School of Engineering

Journal Name

ARTICLE

Controlling nanowire nucleation and growth with a negative substrate bias

Received 00th January 20xx,
Accepted 00th January 20xx

DOI: 10.1039/x0xx00000x

www.rsc.org/

J. Ball and H. S. Reehal

The varied applications of silicon nanowires can influence the required wire density, diameter and length. We demonstrate the ability to control wire nucleation, diameter and length with the use of a negative substrate bias generated with the application of a RF signal in an electron cyclotron resonance chemical vapour deposition system. Growing nanowires from 0 V to -100 V bias we observe trends in the density, length and diameter in wires grown from two different thicknesses of Au. A model for the observed results is suggested.

Introduction

Semiconductor nanowires have potential applications across a variety of fields such as sensors [1,2] biochemical applications [3,4] and solar energy [5,6,7]. Methods of wire fabrication vary with the semiconductor material and end use, with wire structure affecting device functionality. Silicon is a common choice of material due to the suitability of the material for a wide range of potential applications [8,9], low cost and variety of deposition methods. Traditionally Si nanowires (SiNW) are grown via the vapour-liquid-solid (VLS) effect [10] by chemical vapour deposition (CVD) from Si carrier gasses such as SiH_4 [11,12], SiH6 [13] and H_2:$SiCl_4$ [14]. Plasma enhanced CVD (PECVD) has also been used to grow SiNW on both Si substrates [15] and low cost alternatives such as glass [16].

SiNW grown using the VLS method require a catalyst metal forming nucleation sites for the subsequent wire growth. Traditionally, Au has been used although other metals including Cu [17], Sn [18], Bi [19] and In [20] have also been studied. Choice of metal for the catalyst particles has an influence on deposition conditions and wire structure. Low tension metals such as Sn and Bi have the advantage of a low eutectic point with Si, thus wires can be grown at temperatures lower than required for high tension metals such as Au and Cu but require PECVD to achieve successful growth. These typically require growth temperatures in the region of 500°C-600°C for kink free wires grown from Au with SiH_4 [21] to temperatures >900°C for wires grown from Cu and Au with H_2:$SiCl_4$ [22].

Varied growth conditions, catalyst metals, gas precursors and temperatures yield a wide range of SiNW crystal qualities. Low tension metals tend to produce SiNW with twins and dislocations [23,24] while varying the process pressure in Au catalysed growth can lead to kinked wires [25]. SiNW grown from Au metal layers using PECVD and a RF source have demonstrated increased growth rate and a tapered morphology [26]. PECVD operates at process pressures in the low Torr range. The growth of SiNW from In [27] and Sn [23] has been demonstrated in the mT range using electron cyclotron resonance CVD (ECRCVD). As an alternative to RF PECVD, this technique provides greater control of ion bombardment along with low flows of process gas. In this paper we present results on the growth of SiNW from Au via ECRCVD under ion bombardment controlled by the application of a RF signal to the substrate holder. This leads to the generation of a negative DC self-bias at the substrate. The influence on SiNW growth of varying the DC self-bias is reported.

Experimental Method

Si (111) substrates were cleaned in electronic grade acetone in an ultrasonic bath and rinsed in deionised water (DI), followed by a N_2 blow dry. The substrates were then subjected to a 'piranha' etch in 3:1 H_2SO_4:H_2O_2 followed by a DI rinse and N_2 blow dry. The native oxide was removed with a 2 minute dip in <2% HF followed by a N_2 blow dry and loading into a KJL PVD 75 ebeam evaporation system. The samples were pumped to 4x10-7 Torr then deposited with either 1.5nm or 3nm thick films of 5N purity Au. The thickness was monitored with a crystal thickness monitor.

The substrates were unloaded and subjected to a 2 minute <2% HF dip prior to loading into the ECRCVD system for either

London South Bank University - Engineering & Design
103 Borough Road London SE1 0AA
United Kingdom
† Footnotes relating to the title and/or authors should appear here.
Electronic Supplementary Information (ESI) available: [details of any supplementary information available should be included here]. See DOI: 10.1039/x0xx00000x

wire growth or particle size analysis. The HF dips have been identified by Lugstein et.al. [28] as an essential step in SiNW growth. They observed that a dip prior to Au deposition and prior to wire growth removed the native Si oxide. This oxide forms on the Si wafer and diffuses through the Au surface inhibiting wire growth. Due to the lack of affect HF has on Au [29] at ambient temperatures we expect no influence on the as formed Au layers from this surface preparation step.

The ECRCVD system had a base pressure of $2.3x10^{-7}$ Torr and used a Roth and Rau 250PQ ECR source. Samples for particle analysis were ramped to deposition temperature as given in Table 1 in 60 minutes, the heater was turned off and samples removed. Samples for wire growth were ramped to deposition temperate in 60 minutes, then SiNW were grown using SiH_4 with H_2 as the plasma gas.

The ion bombardment was controlled with the generation of a substrate self-bias produced by the application of a RF signal to the substrate holding electrode. Figure 1 shows a schematic of the ECRCVD system with the position of the RF generator.

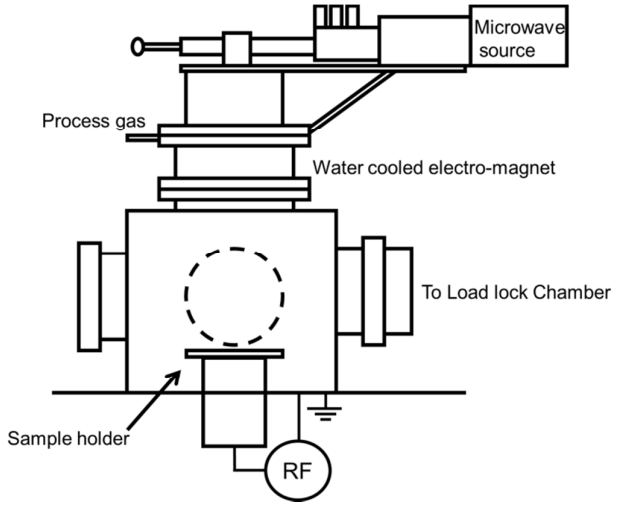

Figure 1: ECRCVD system and RF bias generator.

The Rf bias was generated with an AD-TEK AX 600 supply driving the sample holder at 13.56 MHz with a matching unit to ensure accurate repeatable power transfer. Voltage bias was monitored via a digital display.

The deposition parameters are given in Table 1. Nanowire growth runs had a control Si (111) substrate which had been subjected to the same process steps as those for SiNW growth minus the Au layer. These control samples were masked to allow the formation of a step for film thickness and deposition rate measurement with a Vecco Dektak 6M stylus profilometer.

For selected growth parameters the repeatability of the SiNW growth was tested by preparing multiple samples.

Table 1: Silicon nanowire growth parameters.

Parameter	Value
Process pressure (mT)	10
Temperature (°C)	525
Magnet current (A)	5
Microwave power (W)	800
SiH_4 gas flow (sccm)	3
H_2 gas flow (sccm)	30
Deposition time (min)	15
DC bias (V)	0 to -100

On removal from the ECRCVD system the samples were characterised with a Hitachi S4300 scanning electron microscope (SEM). Wires grown at the various substrate bias regimes were analysed with Image J analysis software from SEM images with the substrate angled at 30° to the incident electron beam. The angled images were taken at 7K magnification and images normal to the substrate at 2.5K magnification, with working distances at 11mm and 9mm, respectively. From the images, the length and diameter were measured by analysing ~100 SiNW per growth regime. Wire length was measured from the base of the wire to the bottom of the catalyst particle whereas the diameter was measured in two places, at the base and just under the particle.

Film structure in the control samples was characterised by studying the crystalline Si 520 cm^{-1} TO phonon mode using Raman spectroscopy. This was done in a Renishaw 2000 system using the 488 nm line of an Ar ion laser.

The catalyst particles formed by annealing prior to deposition were analysed with a Vecco multimode atomic force microscope (AFM) in contact mode and SEM. The SEM images were taken of the as annealed samples at 18K magnification with an area of 35.77 μm^2 and a working distance of 9 mm.

Results

Thin film control samples

The deposition rate as measured on the control samples can be seen in figure 2. The rate appears to increase slightly with increasing negative substrate bias except at -25 V, where it drops significantly by ~35% from~17 to 11 nm/min before recovering again. The Raman spectra of the control samples compared to a Si (111) wafer can be seen in figure 3, with the TO peak parameters listed in Table 2.

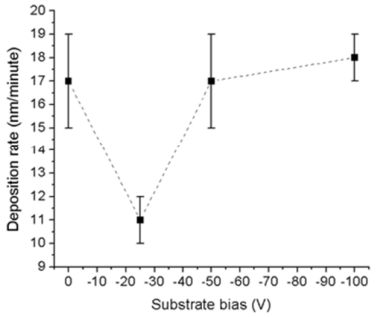

Figure 2: Si deposition rate at varying levels of substrate self-bias. (Dotted line guide to the eye).

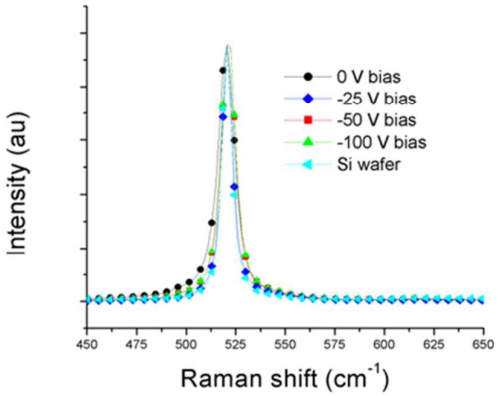

Figure 3: Raman spectra of control samples compared with Si (111) wafer.

The Raman spectra indicate a variation in the film structure with substrate bias as can be seen by the variation in peak position and FWHM when compared to a Si (111) wafer.

Table 2: Raman 520 cm-1 peak parameters

Substrate	Raman peak	FWHM (cm^{-1})
0	520.19	9.50
-25	520.63	6.30
-50	521.24	8.03
-100	521.21	8.30
Si wafer	520.50	5.89

The film grown at 0 V bias deviates the greatest in FWHM while that grown at -25 V shows the greatest similarity to the Si wafer. Samples grown at -50 and -100 V give very similar Raman spectra, in between those grown at 0 V bias and the -25 V Si wafer readings, although these films indicate a greater degree of compressive stress judging from the peak position.

Catalyst particle size

The size of the initial catalyst particle has an influence on the diameter of the resulting nanowire [30]. Analysing the images with Image J analysis software determined the mean particle diameter for the 3nm initial Au layer as 84 nm ± 5 nm with a maximum size of 250 nm ± 18 nm. The 1.5 nm Au layer had a mean diameter of 59 nm ± 2 nm with a maximum diameter of 184nm ± 11 nm. The density of the initial Au particles determined from Image J analysis was 16 ± 2 /μm^2 for the 3nm layer and 14 ± 1 /μm^2 for the 1.5nm layer. AFM images of the particles formed from the 1.5nm and 3nm Au layers prior to deposition can be seen in figure 4.

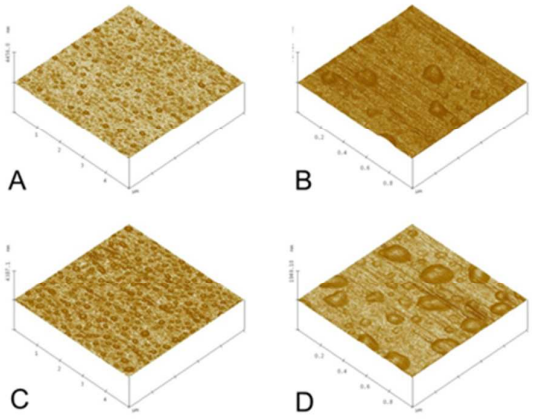

Figure 4: AFM images of Au catalyst particles formed prior to wire growth. (a) initial 1.5nm (5 x 5 µm area) (b) initial 1.5 nm Au (1 x 1 µm area) (c) initial 3 nm (5 x 5 µm area) (d) initial 3 nm Au (1 x 1 µm area).

The particles formed from the 1.5 nm thick layer are shown in figure 3 A and B and those from the 3nm layer in 3 C and D. The particle sizes and distributions are broadly consistent with the results from the Image J analysis. The 3nm layer exhibits larger particles compared to the 1.5nm layer with densities that are similar but with a slightly greater number formed from the 3nm layer, along with larger particles as expected.

SiNW density

The variation of SiNW density with negative DC substrate bias is shown in figure 5 (a) for growth from 3nm thick initial Au layers. It can be seen that wire density increases from 0 V to -50 V. However, further negative bias (-100V) leads to a significant drop off in density to below the 0 V bias level.

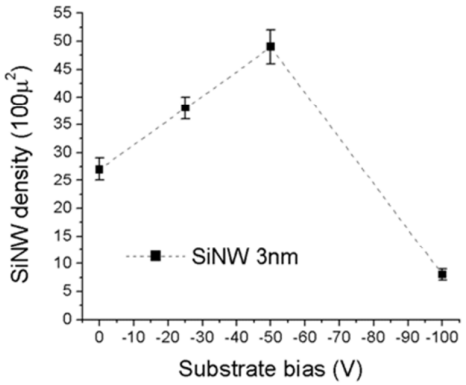

(a)

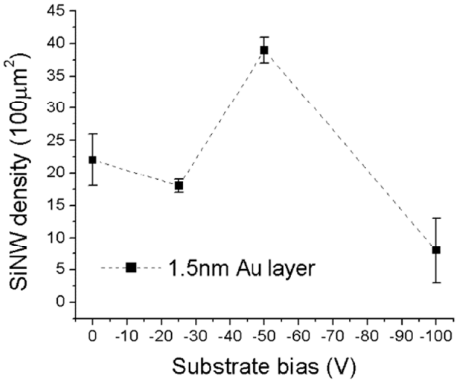

(b)

Figure 5: SiNW density with changing levels of voltage bias grown from (a) the 3 nm initial Au layer and (b) the 1.5 nm initial Au layer. (dotted line guide to the eye).

The SiNW density for 1.5nm thick initial Au layers is shown in Figure 4 (b). The trend is broadly similar to growth from the 3 nm initial layers. The density at -50 V bias is higher than at 0 V, although there is also a decline at -25 V bias. A bias of -100 V yields a very low density as for the 3nm initial layers.
The SEM micrographs of Figure 6 (a) and 4 (b) show a pictorial representation of the density variation for growth on the 3 nm and 1.5 nm initial Au layers, respectively.

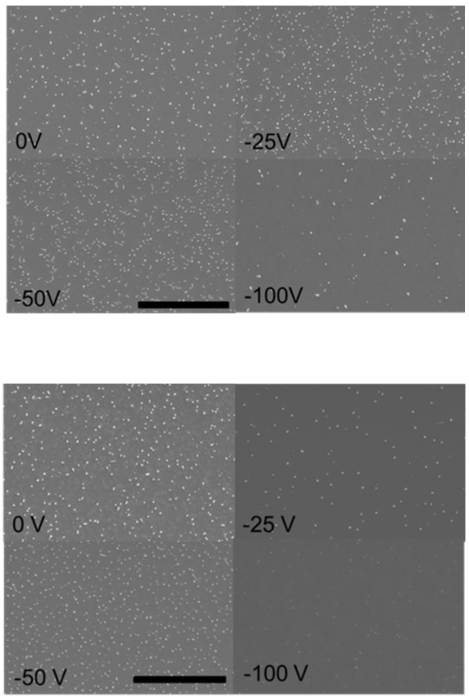

(a)

(b)

Figure 6: SEM images of SiNW at bias levels ranging from 0 to -100V grown from (a) 3 nm initial Au layers (b) 1.5 nm initial Au layers. Scale bar 20 μm.

SiNW length

The length of the SiNW is plotted in figure 7 (a) for growth on the 3 nm initial layer. There is a progressive drop in length from 963 ± 183 nm at 0 V bias to 429 ± 108 nm at -100 V bias. Interestingly, the variation of wire length shows a different trend for growth from the 1.5 nm thick Au layers (figure 5 (b)). Here the length initially increases with bias up to -50 V before showing a significant drop at -100 V. In general, the wire lengths are smaller than for the 3 nm thick initial Au layers.

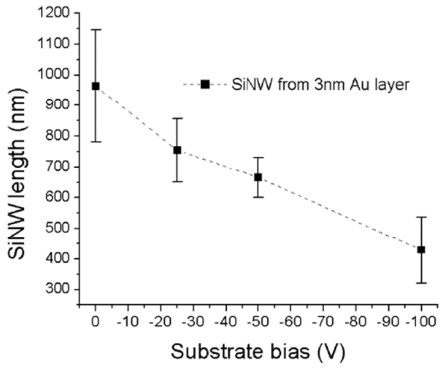

(a)

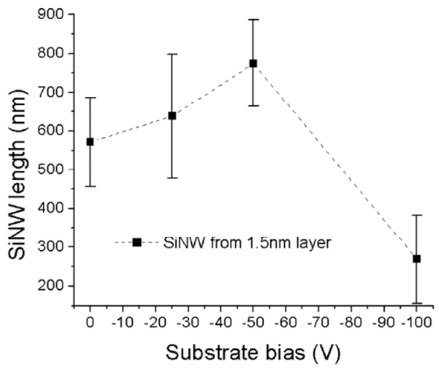

(b)

Figure 7: SiNW length with changing levels of voltage bias for wires grown from (a) 3 nm initial Au layers (b) 1.5 nm initial Au layers (dotted line guide to the eye).

SiNW diameter

Diameter was measured at the base of the wire and under the Au cap. The variation with DC bias is shown in Figure 8.

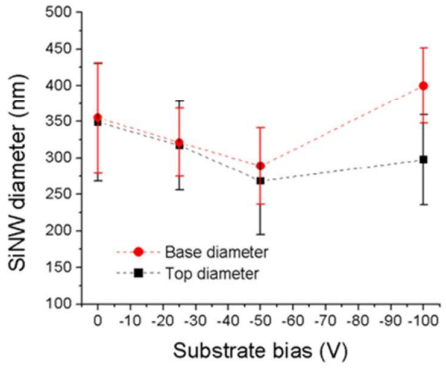

(a)

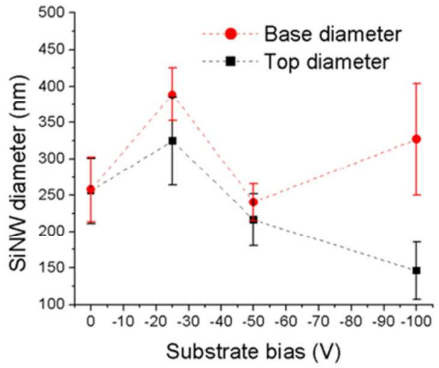

(b)

Figure 8: SiNW diameter with changing levels of voltage bias for growth from (a) 3 nm initial Au layers (b) 1.5 nm initial Au layers (dotted line guide to the eye).

For the 3 nm initial Au layers, the diameter falls with increasing negative bias up to -50 V followed an increase in both base and top diameter at -100 V bias. The wires are essentially parallel at 0 V bias but at -50 V a small taper exists. This increases significantly when the bias increases to -100 V with the top diameter below its value at 0 V bias.

Wires grown from the 1.5 nm thick initial Au layers are also non-tapered at 0 V bias with those grown under a -100 V bias indicating a high level of tapering. With the exception of the data at -25 V bias, the behaviour is broadly similar to that of Figure 7 (a), although the level of tapering at -100V is more extreme.

Examples of parallel and tapered wire growth are shown by the higher resolution SEM images in Figure 9 for the 3nm and 1.5 nm thick initial Au layers.

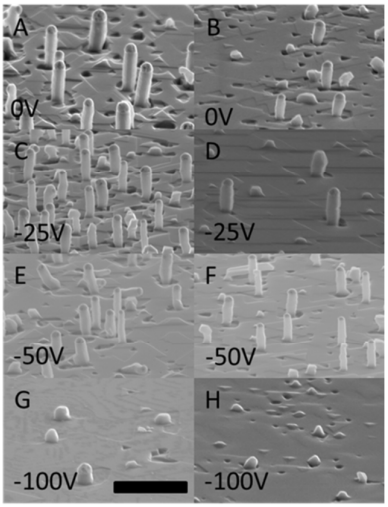

Figure 9: SEM images of SiNW grown from 3 nm Au layers: (A) 0 V, (C) -25 V, (E) -50 V and (G) -100 V. From 1.5 nm Au layers: (B) 0 V, (D) -25 V, (F) -50 V and (H) – 100 V. Scale bar 2µm.

Discussion

The deposition rate of Si on the control sample presented in figure 2 shows little variation with increasing negative bias except in the -25 V growth regime where it shows a significant decrease. Variation in the rate of deposition in both ECRCVD and RF PECVD films grown under a varying bias has been reported by other groups [31, 32]. Kroley [33] observed that deposition rate varied not only with substrate bias but showed variation in the same bias regimes with different gas mixtures. We have also observed a change in deposition rate at this substrate bias at lower temperatures [34]. Interestingly, the lower deposition rate at -25V leads to the optimum film crystallinity as judged by the Raman spectra in figure 3 and Table 1. This variation in material structure with bias has been previously reported in ECRCVD grown films [35, 36, 37].

Reduced ion energy [38] along with positive substrate bias has been found to improve Si film crystallinity in PECVD [39]. While

negative bias has generally been reported as having a detrimental effect [38, 39]. However, exceptions to this have been reported for ECRCVD, for example by DeBoer et. al. [40]. They observed an abrupt change in crystallinity at about -15 V with increases in FWHM and a move of the peak position away from that expected for bulk Si. DeBoer et. al. suggest the ion bombardment changes with substrate bias, while other groups have attributed changes in film structure to changes in the ratio of ions to radicals [41].

ECRCVD decomposes the Si precursor SiH_4 prior to reaching the substrate leading to SiH_3 and SiH_2 radicals, the proportions of which depend on H_2 concentration [42]. Typically SiH_2 Is found to be ~8 times lower in concentration than SiH_3 with even lower levels of SiH and Si [43]. Due to the long mean free path of ECRCVD systems species ion bombardment is perpendicular to the substrate [44]. Increasing the negative bias will accelerate ions towards the substrate increasing the impact energies. This increase in the energy has been suggested to increase surface diffusion [45] and contribute to substrate heating [46].

We suggest that these mechanisms and their interactions with the species produced by ECRCVD may be responsible for the observed changes in deposition rate and film structure.

Turning now to the formation of the initial seed particles on the growth substrates, this shows a dependence on the thickness of the initial Au layer thickness (a comprehensive review on dewetting phenomena has been authored by C.V. Thompson [47]). This difference in particle size is relevant due to the relationship observed between the initial particle and as grown wire diameter by Cui et. al. [30] where the diameter of the SiNW is approximately the diameter of the initial catalyst particle.

The densities of SiNWs seen in figure 5 are significantly lower than the density of initial catalyst particles. The mean/maximum diameter of particles from both initial layers of Au are smaller than the observed respective SiNW diameters in figure 8. The Gibbs-Thomson effect suggests a minimum size at below which nucleation from initial particles cannot take place [48]. We have witnessed this divergence between particle and wire density previously and attribute it to the Gibbs-Thomson effect particle. The majority of Au catalyst particles formed fall below the minimum size required for growth. Those particles that have nucleated have reached the size for growth via agglomeration [23, 49] to a size greater than initially formed, thus yielding SiNW with diameters greater than the initial Au particles.

From figures 7 and 8 it can be seen that the length of wires grown at 0 V bias from both initial Au catalyst layer thicknesses exhibit a diameter dependence, the wires with the greater diameter being longer and thus having a greater growth rate. Typically ascribed to the Gibbs- Thomson effect [48], this is the subject of numerous theoretical discussions such as Roper et.al. [50], Dubrovskii and N.V. Sibirev [51] and Schmidt et.al. [52].

Wires grown from the 3nm Au layer demonstrate a decreasing diameter with increasing negative bias up to -50V, accompanied by a concomitant decrease in growth rate and increase in wire density. This diameter dependant growth suggests the Gibbs-Thomson regime being operative. The increasing density can be explained by the increased number of smaller diameter particles available for nucleation and growth.

This behaviour changes at -100 V bias, where we believe a different growth regime may operate to give sparse, shorter and tapered wires. We suggest two possible reasons. Firstly the increase in wire diameter along with reduced growth rate and density could be due to highly energetic growth species favouring thin film deposition which could reduce the ability of the smaller catalyst particles to nucleate, thereby choking off growth. Secondly the catalyst particles could be subjected to a stronger etch effect from the plasma [26], again inhibiting growth from all but the largest particles. SiNW grown from the 1.5 nm thick layer at -100 V bias exhibit similar behaviour and we suggest similar mechanisms operating.

SiWN grown from the 1.5 nm layer at the -25 and -50 V bias regimes deviate from the trends demonstrated by wires grown from the thicker layer. Growth at -25 V bias with its increased diameter and growth rate suggests diameter dependant growth, coupled with a decrease in density, possibly due to conditions where smaller diameter particles cannot nucleate. However, at -50 V bias, we see an increased density and growth rate with a decrease in diameter which implies a change to diameter independent growth.

Shakthivel and Raghavan [53] have developed a steady state kinetic model for VLS grown nanowires. Their analysis considers four modes of growth (i) layer by layer (LL) at the liquid-solid interface, (ii) LL growth at the triple phase boundary (iii) multi-layer growth (ML) and (iv) rough interface motion (RI). They suggest diameter dependant growth rates require evaporation and reverse reactions to be present and that in most cases the LL growth mode is dominant. However, diameter independence can occur in LL mode if the nucleation rate is inversely proportional to R^2 (radius of the wire). Diameter independent growth is expected, in most conditions, to feature the ML growth mode.

The change in trends observed in the 1.5 nm Au layer at -25 V and -50 V could be attributed, we suggest, in part to a change of growth mode from LL to ML. Growth at 0 V bias shows diameter dependant growth typical of the Gibbs-Thomson effect which we can suggest is driven by the LL growth mode. Growth from 1.5 nm Au at -25 V bias, we suggest, still follows LL growth but the decrease in deposition rate seen in the control samples in this bias regime favours nucleation from larger catalyst particles. These need to agglomerate to a size from which growth is possible for the specific bias regime, hence the larger wire diameter and lower density.

However, at -50 V the increase in wire density and reduction in diameter suggests a greater number of smaller particles are available for growth. The increase in growth rate observed between -25 V and -50 V from the 1.5nm Au layer we attribute to a change in growth mode, from LL to ML, possibly due to a change in growth conditions discussed above. Growth from 3 nm Au exhibits a similar trend in the 0 to -50 V regimes due to LL growth dominating due to particle size.

Interestingly wires previously grown in our system did not exhibit diameter dependant growth [49]. We attribute this to trace levels of oxygen contamination which have been significantly reduced in the present case due to system modifications resulting in a significantly lower base pressure. A reduction in oxygen has been observed to increase surface diffusion [54, 55], which Shakthivel and Raghavan [53] suggest is compatible with diameter dependent growth.

Conclusions

We have grown SiNW from SiH_4 via the VLS effect by ECRCVD with varying substrate bias from two different initial thicknesses of Au layer. Wires grown from the thicker, 3 nm layer decrease in length with increased substrate bias while exhibiting an increase in density in bias regimes up to -50 V. The diameter of the wires decreases with increasing negative bias with the growth appearing to be diameter dependant as length decreases with decreasing diameter.

The -100 V bias regime is detrimental to SiNW grown from both Au layer thicknesses with the resulting SiNW demonstrating low density growth rate and large diameter wires. Wires from both initial layers exhibit taper especially from the 1.5 nm Au layer. We suggest two possible reasons. Firstly the highly energetic growth species favours thin film deposition reducing the ability of the smaller catalyst particles to nucleate choking off growth. Secondly the catalyst particles could be subjected to an etch effect, again inhibiting growth in all but the largest particles.

SiNW grown from the 1.5 nm layer demonstrate increasing length with increasing negative substrate bias. The -25 V growth regime shows decreasing density with increasing wire diameter, this changes for the -50 V regime with increased density, decreased diameter and further increase in growth rate. While diameter dependant growth is seen for the 0 V, -25 V and -100 V growth regimes we propose that a switch to diameter independent SiNW growth is seen in the change from -25 to -50 V bias. This variation from diameter dependent to diameter independent growth could be influenced by the changes in ion bombardment resulting from the change in substrate bias. The effects of increased surface heating [47] and surface diffusion of species [46] we suggest could alter the growth mode from LL to ML.

These results suggest that the change in substrate bias in conjunction with initial catalyst layer thickness can be utilised to control SiNW density and morphology. It should be noted that the growth of SiNW with a changing substrate bias shows sensitivity to the initial conditions. Our findings show that specific trends in morphology and density can be observed for changing conditions but are difficult to predict. Attention should be paid to initial substrate preparation, Au deposition and bias control. The results presented give an insight into the parameter space of this growth technique and suggest a guide to further investigation.

References

1 F. Patolsky and C. M. Lieber, *Materials Today*, 2005, **8**, 20.
2 A. O. Niskanen, A. Colli, R. White, H. W. Li, E. Spigone and J. M. Kivioja, *Nanotechnology*, 2011, **22,** 295502.
3 X. Duan, T-M. Fu, J. Liu, C.M. Lieber, *Nano Today*, 2013, **8**, 351.
4 R. Yan, J-H. Park, Y. Choi, C-J. Heo, S-M. Yang, L.P. Lee, P. Yang, *Nature Nanotechnology*, 2012, **7,** 191.
5 M.D. Kelzenberg, D.B. Turner-Evans, M.C. Putnam, S.W. Boettcher, R.M. Briggs, J.Y. Baek, N.S. Lewis and H.A. Atwater, *Energy & Environmental Science*, 2011, **4**, 866.
6 A. D. Mohite, D. E. Perea, S. Singh, S. A. Dayeh, I. H. Campbell, S. T. Picraux, and H. Htoon, *Nano Letters*, 2012, **12**, 1965.
7 C. E. Kendrick, H. P. Yoon,Y. A. Yuwen, G.D. Barber, H. Shen, T.E. Mallouk, E.C. Dickey, T.S. Mayer, and J.M. Redwing, *Applied Physics Letters*, 2010, **97,** 143108.
8 F. Priolo, T. Gregorkiewicz, M. Galli and T.F. Krauss, *Nature Nanotechnology*, 2014, **9**, 19.
9 A.W. van Herwaarden, D.C. van Duyn, B.W. van Oudheusden and P.M. Sarro, *Sensors and Actuators A: Physical*, 1990, **22,** 621.
10 R.S. Wagner and W.C. Ellis, *Transactions of The Metallurgical Society of AIME*, 1965, **233**, 1053.
11 Th. Stelzner, M. Pietsch, G. Andra, F. Falk, E. Ose and S. Christiansen, *Nanotechnology*, 2008, **19**, 295203.
12 S. Perraud, S. Poncet, S. Noel, M. Levis, P. Faucherand, E. Rouviere, P. Thony, C. Jaussaud and R. Delsol, *Solar Energy Materials & Solar Cells*, 2009, **93**, 1568.
13 S. Akhtar, K. Usami, Y. Tsuchiya, H. Mizuta, and Shunri Oda, *Applied Physics Express*, 2008, **1**, 014003.
14 M. C. Putnam, D. B. Turner-Evans, M. D. Kelzenberg, S. W. Boettcher, N. S. Lewis, and H. A. Atwater, Applied Physics Letters, 2009, **95**, 163116 .
15 S. Hofmann, C. Ducati, R. J. Neill, S. Piscanec, and A. C. Ferrari, J. Geng, R. E. Dunin-Borkowski and J. Robertson, *Applied Physics Letters*, 2003, **94**, 6005.
16 J. Ball, A. Centeno, B. G. Mendis, H. S. Reehal and Neil Alford, *Optics Express*, 2012, **20,** 20266.
17 M.C. Putnam, D. B. Turner-Evans, M.D. Kelzenberg, S.W. Boettcher, N.S. Lewis and H.A. Atwater, *Applied Physics Letters*, 2009, **95**, 163116.
18 M.S. Jeon and K. Kamisako, *Materials Letters*, 2009, **63**, 777.
19 L. Yu, F. Fortuna, B. O'Donnell, T. Jeon, M. Foldyna, G. Picardi and P. Roca i Cabarrocas, *Nano Letters*, 2012, **12**, 4153.
20 I. Zardo, S. Conesa-Boj, S. Estrade, L. Yu, F. Peiro, P. Roca i Cabarrocas, J.R. Morante, J. Arbiol and A. Fontcuberta i Morral, *Applied Physics A; Materials Science & Processing*, 2010, **100**, 287.
21 J. Westwater, D.P. Gosain, S. Tomiya and S. Usui, *Journal of Vacuum Science & Technology B*, 1997, **15**, 554.
22 B. M. Kayes, M. A. Filler, M. C. Putnam, M. D. Kelzenberg, N. S. Lewis, and H. A. Atwater, 'Applied Physics Letters', 91, (2007). 103110.
23 J. Ball, L. Bowen, B.G. Mendis and H.S. Reehal, *Crystal Engineering Communications*, 2013, **15**, 3808.
24 L. Yu, B.O'Donnell, P-J. Alet, S. Conesa-Boi, F. Peiro and P. Roca i Cabarrocas, *Nanotechnology*, 2009, **20**, 225604.
25 Y-J. Hyun, A. Lugstein, M. Steinmair, E. Bertagnolli and P. Pongratz, *Nanotechnology*, 2009, **20**, 125611.
26 A. Colli, A. Fasoli, P. Beecher, P. Servati, S. Pisana, Y. Fu, A. J. Flewitt, W. I. Milne, J. Robertson,C. Ducati S. De

Franceschi, S. Hofmann and A. C. Ferrari, *Journal of Applied Physics*, 2007, **102**, 034302.
27 M.J. Hernandez, M. Cervera, E. Ruiz, J.L. Pau, J. Piqueras, M. Avella, J. Jimenez, *Nanotechnology*, 2010, **21**, 455602.
28 A. Lugstein, Y.J. Hyun, M. Steinmair, B. Dielacher, G. Hauer and E. Bertagnolli Nanotechnology, 2008, **19**, 485606.
29 'Handbook of Corrosion Data' Editor: B. Craig and D. Anderson, ASM International, 1995.
30 Y.Cui, L.J. Lauhon, M.S. Gudiksen, J. Wang and C.M. Lieber, *Applied Physics Letters*, 2001, **78,** 2214.
31 D. Raha and D. Das, *Solar Energy Materials & Solar Cells*, 2011, **95**, 3181.
32 Yong Liu, PhD Thesis, Iowa State University, (2002).
33 Laurent Kroely, PhD Thesis, Ecole Polytechnique,(2010).
34 J. Ball, B.G. Mendis and H.S. Reehal, *Journal of Materials Science,* 2014, **49,** 2078.
35 A. Matsuda, K. Kumagai and K. Tanaka, *Japanese Journal Applied Physics*, 1983, **22,** L34.
36 W.J. Varhue, J.L. Rogers, P.S. Andry and E. Adams, *Applied. Physics Letters*, 1966, **68,** 349.
37 H. Jia, J. K Saha, N. Ohse and H. Shirai, *Journal of Physics D: Applied. Physics*, 2006, **39,** 3844.
38 M. Kondo and A. Matsuda, *Thin Solid Films*, 2001, **383,** 1.
39 R. Nozawa, H. Takeda, M. Ito, M. Hori and T. Goto, Journal of Applied Physics, 1997, 81, 8035.
40 S.J. DeBoer, V.L. Dalal, G Chumanov and R. Bartels, Applied Physics Letters, 1995, 66, 2528.
41 J. K. Rath, Solar Energy Materials and Solar Cells, 2003, 76, 431.
42 H. L. Hsiao, H.L. Hwang, A.B. Yang, L.W. Chen and T.R. Yew, App. Surf. Sci., 1999, **142**, 1.
43 V.L. Dalal, T. Maxson, K.Han and D. Haroona, Journal of Non-Crystalline Solids, 1998, **2**, 227.
44 J. Asmussen, IEEE Transactions on Plasma Science, 25, (1997), 1196.
45 J.Perrin, in: Plasma Deposition of Amorphous Silicon Based Materials, ed. G. Bruno, P. Capezzuto and A. Madan, London, Academic Press, 1995.
46 K. B. K. Teo, D. B. Hash, R. G. Lacerda, N. L. Rupesinghe, M. S. Bell, S. H. Dalal, D. Bose, T. R. Govindan, B. A. Cruden, M. Chhowalla, G. A. J. Amaratunga, M. Meyyappan, and William I. Milne, Nano Letters, 4, (2004), 921.
47 C.V. Thompson, *Annual Review Materials Research*, 42, (2012), 399.
48 E.I. Givargizov, Journal of Crystal. Growth 31 (1975), 20.
49 J. Ball and H.S. Reehal, *Thin Solid Films*, 2012, **520,** 2467.
50 S.M. Roper, S.H. Davis, S.A. Norris, A.A. Golovin, P.W. Voorhees, and M. Weiss*, Journal of Applied Physics*, 2007, **102**, 034304.
51 V.G. Dubrovskii and N.V. Sibirev, *Journal of Crystal Growth*, 2007, **304**, 504.
52 V. Schmidt, J.V. Wittemann and U. Gosele, *Chemistry Review*, 2010, **110**, 361.
53 D. Shakthivel and S. Raghavan, *Journal of Applied Physics*, 2012, **112**, 024317.
54 S. Kodambaka, J.B. Hannon, R.M. Tromp and F.M. Ross, *Nano Letters*, 2006, **6**, 1292.
55 B. J. Kim, J. Tersoff, S. Kodambaka, Ja-Soon Jang, E. A. Stach, and F. M. Ross, *Nano Letters*, 2014, **14**, 4554.